Proteomic analysis of a murine model of lung hypoplasia induced by oligohydramnios

Running Title: **Oligohydramnios affects AKT1, SP-D and CD200 expression**

Tanbir Najrana[1,2,] Nagib Ahsan[3,4], Rasha Abu-Eid[5], Alper Uzun[1,6], Lelia Noble[7], George Tollefson[1] and Juan Sanchez-Esteban[1]

[1]Department of Pediatrics, Women and Infants Hospital/Warren Alpert Medical School of Brown University, Providence, RI, USA

[2]Department of Pathology and Laboratory Medicine, Brown University, Providence, RI 02903 USA

[3]Department of Chemistry and Biochemistry, Stephenson Life Sciences Research Center, University of Oklahoma, Norman, Oklahoma, 73019

[4]Mass Spectrometry, Proteomics and Metabolomic Core Facility, Stephenson Life Sciences Research Center, University of Oklahoma, Norman, Oklahoma, 73019

[5]Institute of Dentistry, School of Medicine, Medical Sciences & Nutrition, University of Aberdeen, Foresterhill, AB25 2ZD, UK

[6]Center of Computational Molecular Biology, Brown University, Providence, RI 02906, USA

[7]COBRE Center for Cancer Research Development, Proteomics Core Facility, Rhode Island Hospital, Providence, RI 02903, USA

Address correspondence to: Tanbir Najrana, PhD.
Department of Pathology and Laboratory Medicine
Warren Alpert Medical School
Brown University
55 Claverick Street
Providence, RI 02903, USA

E-mail: tanbir_najrana1@brown.edu

Acknowledgments

This work was supported by funding from the National Institute of General Medical Sciences of the National Institutes of Health, Number: P30GM114750 and Oh–Zopfi Grant for Perinatal Research, Department of Pediatrics; Kilguss Research Core at Women & Infants Hospital of Rhode Island.

Conflict of Interest Statement: The authors declare that there are no conflicts of interest in the authorship or publication of this manuscript.

ABSTRACT

Severe oligohydramnios (OH) due to prolonged loss of amniotic fluid can cause pulmonary hypoplasia. Animal model of pulmonary hypoplasia induced by amniotic fluid drainage is partly attributed to changes in mechanical compression of the lung. Although numerous studies on OH-model have demonstrated changes in several individual proteins, however the underlying mechanisms for interrupting normal lung development in response to decrease of amniotic fluid volume is not fully understood. In this study, we used a proteomic approach to explore differences in the expression of a wide-range of proteins after induction of OH in a mouse model of pulmonary hypoplasia to find out the signaling/molecular pathways involve in fetal lung development. Liquid Chromatography-MassSpectromery/MassSpectrometry (LC-MS/MS) analysis found 474 proteins that were differentially expressed in OH induced hypoplastic lungs in comparison to untouched (UnT) control. Among these proteins, we confirmed the downregulation of AKT1, SP-D and CD200, and provided proof-of-concept for the first time about the potential role that these proteins could play in fetal lung development.

Keywords: Lung, mouse model, oligohydramnios, AKT1, SP-D

INTRODUCTION

Mechanical forces are critical for fetal lung development [1]. The fetus secretes fluid into the lumen of the lung creating a constant transpulmonary pressure that is critical for normal lung development [2]. Tracheal ligation in fetal sheep increased lung distension and promoted lung development; whereas the opposite effect was observed when tracheal lung fluid was drained [3]. These studies clearly suggest that mechanical forces secondary to fluid distention are a major determinant for fetal lung growth.

Underdevelopment of the lung, or pulmonary hypoplasia, is a common finding in neonatal autopsies (around 22%) [4]. Oligohydramnios (OH), congenital diaphragmatic hernia and renal agenesis are major causes of pulmonary hypoplasia and neonatal mortality and morbidity. OH is a state in which the volume of amniotic fluid surrounding the fetus *in utero* is substantially decreased. The sources of amniotic fluid are maternal plasma, fetal membrane, and fetal urine, when fetal kidneys start to function. In humans, rupture of the fetal membrane can cause OH [5]. In an experimental model, we and others have shown the induction of pulmonary hypoplasia by amniotic fluid drainage in the canalicular stages of lung development [6-8]. The likely mechanism is a reduction in the distention of the lung secondary to a decrease of the volume of fluid in the potential airways and air spaces [9-11]. However, the molecular mechanisms by which a decrease of lung distention compromises lung development are not well understood.

Prior studies have demonstrated that several factors are involved in lung development. For example, in a rat model of OH induced at the pseudoglandular stage of lung development, the crucial role of platelet-derived growth factor (PDGF) and its receptors for alveolarization during normal lung development was demonstrated [12]. Altered extracellular matrix caused by OH might

correspond to altered respiratory function of the offspring [13]. Indeed, in hypoplastic human fetal lungs, the absence of elastic tissue is associated with maternal OH [14]. Furthermore, OH induced at the pseudoglandular stage of lung development in rat showed decreased expression of collagen I [15]. All together, these studies indicate an important role of extracellular matrix in lung development mediated by mechanical signals.

Vascular endothelial growth factor (VEGF) plays an important role in endothelial cell differentiation and angiogenesis. However, in a fetal rat model of OH, angiogenesis was compromised without affecting the expression of VEGF [13]. These studies suggest that, in addition to VEGF, other angiogenic factors may be involved in regulating fetal lung angiogenesis. These studies also emphasize the complexity of fetal lung angiogenesis.

In order to better understand the differentially expressed proteins in a mouse pulmonary hypoplasia model, we used a proteomic approach as a system-based screening method. The present investigations are a continuation of our previous studies [6] with the long-term goal of elucidating the underlying mechanism of lung development mediated by mechanical forces.

This study provides a wealth of information to investigate the underlying cellular and molecular mechanism of the development of the lung associated with mechanical force.

MATERIAL AND METHODS

Animal Experiment to induce Oligohydramnios (OH)

Surgical procedures used in this study were approved by the Lifespan Institutional Animal Care and Use Committee (IACUC) of Rhode Island. We followed the procedure to induce pulmonary hypoplasia on mice by OH as previously described [6]. Frozen lungs were submitted to COBRE Center for Cancer Research Development Proteomics Core Facility of Rhode Island Hospital, Providence, RI to use for the proteomics analysis. Detailed methods of OH induction in animal experiment is provided in supplementary file 1.

LC-MS/MS

The LC-MS/MS analysis was performed on a fully automated proteomic technology platform that includes an Agilent 1200 Series Quaternary HPLC system (Agilent Technologies, Santa Clara, CA) connected to a Q Exactive Plus mass spectrometer (Thermo Fisher Scientific, Waltham, MA). The LC-MS/MS set up was used as described earlier [16]. The MS/MS spectra were acquired at a resolution of 17,500, with a targeted value of 2×10^6 ions or maximum integration time of 200 ms. The ion selection abundance threshold was set at 8.0×10^2 with charge state exclusion of unassigned and z =1, or 6-8 ions and dynamic exclusion time of 30 seconds.

Database search and label-free quantitative analysis

Peptide spectrum matching of LC-MS/MS spectra of each file was searched against the Uniport *Mus musculus* database (TaxonID: 10090, downloaded on 02/09/2015) using the SEQUEST algorithm within Proteome Discoverer v 2.3 software (Thermo Fisher Scientific, San Jose, CA). The SEQUEST database search was performed with the following parameters: trypsin enzyme cleavage specificity, 2 possible missed cleavages, 10 ppm mass tolerance for precursor ions, 0.02 Da mass tolerance for fragment ions. Search parameters permitted dynamic modification of

methionine oxidation (+15.9949 Da) and static modification of carbamidomethylation (+57.0215 Da) on cysteine. Peptide assignment from the database search was filtered down to a 1% FDR. The relative label-free quantitative and comparative among the samples were performed using the Minora algorithm and the adjoining bioinformatics tools of the Proteome Discoverer 2.3 software. To select proteins that show a statistically significant change in abundance between two groups, a threshold of 1.5-fold change with p-value (0.05) were selected. Proteomics data is submitted in public repository (MassIVE MSV 000086641).

Bioinformatics analysis

The proteomic dataset was further analyzed by the adjoining tools of the Proteome Discoverer v2.3 software. The gene enrichment analysis including KEGG and WiKi pathway analysis of the significantly abundant proteins was conducted with an open source bioinformatics platform named ShinyGO (http://bioinformatics.sdstate.edu/go/). STRING, an open source protein-protein interaction network was used to develop our protein of interest network.

Statistics analysis

Student t-test or Mann Whitney test (GraphPad prism software, Version 5.04) were used for statistical analyses to identify differences between control and OH tissues. $P \leq 0.05$ was considered statistically significant

Further details of the methodology are described in the supplementary materials.

RESULTS

1. Model of pulmonary hypoplasia

To confirm the presence of pulmonary hypoplasia in OH lungs, morphometric analysis was performed on H&E stained histological sections. Our results confirmed our previous findings [6], and clearly showed a significant reduction in lung space size as measured by area and perimeter (Figure 1 A, B and C).

We also tested the reproducibility of the expression of T1 alpha and SP-C (alveolar epithelial cell type I (AEC1) and type II (AEC2) markers respectively), and EMCN (endomucin, endothelial cell marker) proteins in OH lung, as a justification of using the mouse model (Figure 1D). A representative immunoblot shows that the expression of T1 alpha, and EMCN decreased in OH lung when compared to untouched controls (UnT) whereas the abundance of SP-C protein did not change. These studies validate the pulmonary hypoplasia mouse model, as we have previously reported [6]. Tissues from these lungs were used to carry out the proteomic analysis in this study.

2. Identification of differentially expressed proteins in oligohydramnios induced pulmonary hypoplasia

A comparative label-free relative quantitative proteomic analysis was performed between UnT and OH lungs. Three biological replicates were used in each group of samples. A total of 23587 unique peptides corresponding to 3385 unique proteins were identified by LC-MS/MS analysis. Principal component analysis (PCA) demonstrated comparatively close clustering of total normalized protein abundance among the replicates in each condition with a clear distinction between the conditions (parabolic structures; light orange, UnT & light blue, OH) (Figure 2A**)**. The total number of unique protein set (3385) identified by LC-MS/MS analysis was further subjected for label free quantitative analysis. A total of 134 and 340 proteins were found to be increased and decreased respectively in abundance at least -2 to 2 folds with significant p-value ($\leq$0.05) in OH

lungs compared to UnT . In volcano plot, x-axis and y-axis represent the differentially expressed proteins with fold changes and statistical significance ($-\log_{10}$ of p value) respectively (Figure 2B**)**. Profiles of differentially expressed proteins are shown using clustering method by generating a heat map. Proteins were grouped based on their similarity of expression pattern and is shown in a grid where each row and column represent protein and sample respectively. Fold change of protein expression was set up at ≤ -1.5 to ≥ 1.5 and p-value at ≤ 0.05. Red and green colors indicate up and down regulation of protein expression respectively (Figure 2C**)**. A closer view of a group of proteins that have similar expression patterns in each condition in all three replicates regardless of any outliers **(**Figure 2D**)**.

3. Classification and pathway analysis of differentially abundant proteins

Pathway enrichment analysis was performed using differentially expressed proteins in OH lungs to identify the enriched affected biological pathways. KEGG and Wiki pathway analysis for 340 downregulated proteins revealed that Apelin signaling and EGF/EGFR signaling are major enriched pathways respectively (Figure 3A and 3B, right panel). These pathways are involved in several cellular processes including cell proliferation, survival, differentiation and angiogenesis [17]. Akt1 gene is involved in the majority of the enriched signaling pathways. Huntington disease and signal transduction S1P receptor pathways are enriched as most affected by 134 upregulated proteins in OH lung by KEGG and Wiki pathway analysis respectively (Figure 3A and 3B, left panel).

4. Verification of proteomic data

A specific group of candidate proteins important for fetal lung development were selected to verify the proteomic dataset. These included AKT1. SP-D and CD200.

AKT pathway plays a role in fetal lung development [18]. AKT1, AKT2 and AKT3 are the three isoforms of AKT. Each isoform has unique and overlapping functions in the regulation of cellular

proliferation, differentiation, apoptosis, and survival [19]. The role of specific AKT isoforms in lung development has not been investigated. Pathway enriched analysis in this study revealed the involvement of AKT1 isoform in most of the signaling pathways affected in oligohydramnios induced hypoplastic lung compared to the control.

There are four surfactant associated proteins; namely SP-A, SP-B, SP-C and SP-D. Among them SP-C is expressed exclusively in AEC2 in the lung and is known as a canonical marker of this cell [20]. In this study, the LC-MS/MS data revealed that among the four surfactant proteins, SP-D was significantly downregulated in OH lung. SP-D protein is well-known as a modulator of lung inflammation [21]. Our data showed that there is no differential expression of any pro-inflammatory factors in the proteomic dataset suggesting that an inflammatory response in OH lung is not activated. Thus, our proteomic data suggest the potential role of SP-D in fetal lung development independent of its role in inflammation.

The proteomics data in this study showed also a significant reduction of CD200 expression in OH lung compare to UnT suggesting the potential role of CD200 in fetal lung development. CD200 is widely spread in both pulmonary and non-pulmonary tissues. CD200 participates in autoimmune and allergic disorders, bone development and reproductive biology [22]. Developmental regulation of CD200 in rat lung has been documented [23] suggesting CD200 has a potential role in OH-induced pulmonary hypoplasia.

Based on our findings, where the proteomic analyses showed significant changes in these proteins, in addition to the above discussion describing the potential role of AKT1, SP-D and CD200, we sought to validate the proteomic data quantitatively using western blot (Figure 4) and IHC (Figure 5).

Figure 4A and 4B represent the immunoblotting and densitometry analysis respectively. Western blot confirmed the proteomic results by showing the significant decrease in the expression of AKT1 ($p \leq 0.05$), SP-D ($p \leq 0.001$) and CD200 ($p \leq 0.05$) in OH compared to UnT lung. AKT2 was used in this assay to test whether AKT1 was the AKT isoform specifically downregulated in OH lung.

IHC also showed reduced expression of AKT1, SP-D and CD200 in OH lung tissue compared to UnT (Figure 5A, D and G). Representative microscopic images of IHC stained sections to detect AKT1, SP-D and CD200 are shown in Figure 5B, 5E and 5H respectively. Figure 5C, 5F and 5I represent the quantitative analysis of the AKT1, SP-D and CD200 expressing positive cells respectively as analyzed by QuPath. Image analysis showed that the percentage of positive cells is significantly decreased for AKT1 ($p<0.0001$), SP-D ($p<0.05$) and CD200 ($p<0.05$) in OH compared to UnT lung. Optical density as a measure of protein expression level was also significantly reduced for AKT1 ($p<0.0001$), SP-D ($p<0.0001$) and CD200 ($p<0.0001$) in both the nuclei and the whole cells. Figure 5 shows representative subsets of the original images, while image analysis was performed on the whole images (representative figures in supplementary file 2).

DISCUSSION

Pulmonary hypoplasia secondary to OH can cause significant morbidity and mortality to the neonatal population [5]. The precise mechanism by which OH induces lung hypoplasia remains unknown. In this study, we used LC-MS/MS proteomic analysis to elucidate the differences in the lung proteomic profile between OH induced lung hypoplasia and UnT control. Our data identified a total of 474 proteins that were significantly differentially expressed in our experimental mouse model of lung hypoplasia including AKT1, SP-D and CD200. Further analysis of the 340 downregulated proteins using KEGG and Wiki enrichments showed that the major significant enriched pathways were the Apelin and EGF/EGFR signaling pathways. Both of these signaling pathways are involved in cell proliferation, differentiation and survival [24-26]. Due to the large data set of differentially expressed proteins in OH lung, here we considered the down regulated proteins to avoid intricacy in the investigation in this study. Full list of significantly down and up regulated proteins are provided in supplementary data file 3. We believe these studies provide novel information on the potential mechanisms underlying lung development mediated by mechanical signals.

Apelin binding to apelin receptors transduces signals through G protein to a variety of signaling pathways including the PI3K-AKT pathway. PI3K-AKT pathway contributes to cell proliferation, survival and differentiation in the development of the fetal murine lung [18]. However, the role of specific AKT isoforms in lung development is not known. Our proteomic data revealed significant down regulation of AKT1 in OH induced hypoplastic fetal mouse lung which was confirmed by western blot and IHC. Akt1 gene is involved in most of the pathways enriched by KEGG analysis including thermogenesis, non-alcoholic fatty liver disease, thyroid hormone signaling pathway, ErbB signaling pathway, focal adhesion and insulin signaling pathway among others. Our investigations suggest that the pathways mediated by AKT1 may be critical in the

pathogenesis of the developmental lung defect in response to OH. On the other hand, our western data revealed no changes in the AKT2 isoform in OH compared to UnT lungs, thus suggesting unique roles for different isoforms in lung development.

Alveolar epithelial cells type 1 (AEC1) and type II (AEC2) differentiation is a hallmark of the development of fetal lung [27]. We had previously described in a murine model of pulmonary hypoplasia, that the decrease of external compression secondary to severe OH can compromise the differentiation of AEC1 cells in the distal lung [6]. In this study, proteomic analysis revealed that the expression of PDK1 is significantly down regulated in OH lung, suggesting a role of PI3K-AKT pathway in lung development. This is an interesting finding, as AKT1 investigations have primarily focused on cancer research with only few studies looking at the role of AKT1 in adipose tissue [28] and mammary gland development [29]. Thus, we speculate that PI3K/PDk1- AKT signaling pathway may be important for ACE1 cell differentiation mediated by mechanical signals. Testing this hypothesis will be the focus of future studies.

Among the four proteins associated with alveolar surfactant namely SP-A, SP-B, SP-C and SP-D, SP-C is known to be a canonical differentiation marker of alveolar AEC2 with its expression restricted to these cells [30]. SP-D is expressed in different cells including non-pulmonary tissues [20]. Our proteomic data revealed a significant down regulation of SP-D in OH lung, which was confirmed by western blot and IHC. The expression of SP-D is gradually increased, and distribution of this protein within the lung changes with the advancing gestation, where it is initially expressed in bronchial epithelial cells and later found in AEC2. But in lungs from patients with bronchopulmonary dysplasia, SP-D was barely detected [31]. These data suggest an important role for this protein during lung development. SP-D is thought to play a role in surfactant homeostasis through unidentified signaling pathways [32]. SP-D is a member of C-type lectin family.

This protein is believed to participate only in innate immunity or non-antibody mediated host defense system in the lung due to its structural feature of collectins [21]. Studies have provided evidence that in addition to their role in innate immunity, collectins could have other functions [33]. Thus, SP-D seems to have other roles in addition to immunity, including a role in lung development as our findings suggest. In this study, the surgical procedure for the induction of OH did not trigger inflammatory signals in the fetal lung as evidenced by the proteomic analysis that did not show differential expression of any key pro-inflammatory cytokines. Thus, down regulation of SP-D in OH lung indicates a potential role in lung development independent of its role in immunity.

CD200 is a membrane glycoprotein that functions as an immunosuppressive signaling molecule [34]. CD200 is widely spread in both pulmonary and non-pulmonary tissues and cells [22.] In the lung, CD200 is expressed on AEC2, Clara cells and endothelial cells. CD200 has a dynamic expression in the developing lung and is associated with alveolar capillary development in rat lung [23]. Here, our results by proteomics analysis and further confirmed by western blot and IHC, revealed the down regulation of CD200 in a pulmonary hypoplasia mouse model. Furthermore, there is a reduction of lung angiogenesis, as previously demonstrated [6]. Together these findings suggest a potential role for CD200 in angiogenesis within the developing lung. This hypothesis needs to be tested experimentally.

Although changes in the expression of AKT1[35,36], CD200[37] and SP-D [38,39] were observed in multiple pulmonary disorders, including lung fibrosis, BPD, RDS, Asthma, COPD and lung cancer, however, the role of these proteins in lung development has not been explored. To our knowledge, this is the first study to report changes in these three proteins in the developing lung as a consequence of OH**.**

Using STRING (protein-protein interaction networks), we identified potential interactions among the significantly downregulated proteins and transcriptional regulators (Figure 6). Lung development is a complicated process, and depends on the timely interplay of highly regulated molecular signals [40]. For example, TFAM (transcription factor A, mitochondrial) is a nuclear gene critical for transcription of the mitochondrial genome [41], and is required for lung development [42]. In protein-protein interaction networks, TFAM is present in an interaction clustered with a central molecule, AKT1. This could indicate its potential role in lung development via AKT-pathway. Another example, is the direct binding of SP-D with MFAP4 (microfibrillar associated protein 4) an extracellular glycoprotein thought to facilitate surfactant homeostasis [43,44] in normal physiological condition. Therefore, protein-protein interaction networks provide a wealth of information which could be used to elucidate unknown mechanisms regulating lung development related to mechanical forces.

In summary, our data revealed significant changes in the expression of a wide variety of proteins as a result of OH induced pulmonary hypoplasia. Our findings show for the first time that AKT1, SP-D and CD200 have potential roles in fetal lung development. This investigation also provided a proof-of-concept that one of the potential mechanisms by which mechanical signals are transduced to physiological signals is through the AKT-pathway with specific isoforms having different functions. The information gained from this study will provide the basis for future investigations to test the role of specific molecules and signaling pathways in fetal lung development. Understanding the mechanisms regulating lung development could lead to the development of new therapies to treat pulmonary hypoplasia.

References

1. Kitterman JA. The effects of mechanical forces on fetal lung growth. *Clin Perinatol.* 1996;23(4):727-740.
2. Hooper SB, Harding R. Fetal lung liquid: a major determinant of the growth and functional development of the fetal lung. *Clin Exp Pharmacol Physiol.* 1995;22(4):235-247.
3. Alcorn D, Adamson TM, Lambert TF, Maloney JE, Ritchie BC, Robinson PM. Morphological effects of chronic tracheal ligation and drainage in the fetal lamb lung. *J Anat.* 1977;123(Pt 3):649-660.
4. Husain AN, Hessel RG. Neonatal pulmonary hypoplasia: an autopsy study of 25 cases. *Pediatr Pathol.* 1993;13(4):475-484.
5. Fliegner JR, Fortune DW, Eggers TR. Premature rupture of the membranes, oligohydramnios and pulmonary hypoplasia. *Aust N Z J Obstet Gynaecol.* 1981;21(2):77-81.
6. Najrana T, Ramos LM, Abu Eid R, Sanchez-Esteban J. Oligohydramnios compromises lung cells size and interferes with epithelial-endothelial development. *Pediatr Pulmonol.* 2017;52(6):746-756.
7. Thibeault DW, Beatty EC, Jr., Hall RT, Bowen SK, O'Neill DH. Neonatal pulmonary hypoplasia with premature rupture of fetal membranes and oligohydramnios. *J Pediatr.* 1985;107(2):273-277.
8. Kitterman JA, Chapin CJ, Vanderbilt JN, et al. Effects of oligohydramnios on lung growth and maturation in the fetal rat. *Am J Physiol Lung Cell Mol Physiol.* 2002;282(3):L431-439.
9. Dickson KA, Harding R. Decline in lung liquid volume and secretion rate during oligohydramnios in fetal sheep. *J Appl Physiol (1985).* 1989;67(6):2401-2407.
10. Savich RD, Guerra FA, Lee CC, Padbury JF, Kitterman JA. Effects of acute oligohydramnios on respiratory system of fetal sheep. *J Appl Physiol (1985).* 1992;73(2):610-617.
11. Cloutier M, Tremblay M, Piedboeuf B. ROCK2 is involved in accelerated fetal lung development induced by in vivo lung distension. *Pediatr Pulmonol.* 2010;45(10):966-976.
12. Chen CM, Wang LF, Chou HC, Lang YD. Oligohydramnios decreases platelet-derived growth factor expression in fetal rat lungs. *Neonatology.* 2007;92(3):187-193.
13. Chen CM, Chou HC, Wang LF, Yeh TF. Effects of maternal retinoic acid administration on lung angiogenesis in oligohydramnios-exposed fetal rats. *Pediatr Neonatol.* 2013;54(2):88-94.
14. Nakamura Y, Fukuda S, Hashimoto T. Pulmonary elastic fibers in normal human development and in pathological conditions. *Pediatr Pathol.* 1990;10(5):689-706.
15. Chen CM, Chou HC, Wang LF, Lang YD. Experimental oligohydramnios decreases collagen in hypoplastic fetal rat lungs. *Exp Biol Med (Maywood).* 2008;233(11):1334-1340.
16. Ahsan N, Belmont J, Chen Z, Clifton JG, Salomon AR. Highly reproducible improved label-free quantitative analysis of cellular phosphoproteome by optimization of LC-MS/MS gradient and analytical column construction. *J Proteomics.* 2017;165:69-74.
17. Datta SR, Brunet A, Greenberg ME. Cellular survival: a play in three Akts. *Genes Dev.* 1999;13(22):2905-2927.
18. Wang J, Ito T, Udaka N, Okudela K, Yazawa T, Kitamura H. PI3K-AKT pathway mediates growth and survival signals during development of fetal mouse lung. *Tissue Cell.* 2005;37(1):25-35.
19. Hers I, Vincent EE, Tavare JM. Akt signalling in health and disease. *Cell Signal.* 2011;23(10):1515-1527.
20. Haagsman HP, Diemel RV. Surfactant-associated proteins: functions and structural variation. *Comp Biochem Physiol A Mol Integr Physiol.* 2001;129(1):91-108.
21. Lu J, Teh C, Kishore U, Reid KB. Collectins and ficolins: sugar pattern recognition molecules of the mammalian innate immune system. *Biochim Biophys Acta.* 2002;1572(2-3):387-400.
22. Gorczynski RM. CD200:CD200R-Mediated Regulation of Immunity. *ISRN Immunology.* 2012;2012:682168.

23. Tsai MH, Chu CC, Wei TS, et al. CD200 in growing rat lungs: developmental expression and control by dexamethasone. *Cell Tissue Res.* 2015;359(3):729-742.
24. Chandra A, Lan S, Zhu J, Siclari VA, Qin L. Epidermal growth factor receptor (EGFR) signaling promotes proliferation and survival in osteoprogenitors by increasing early growth response 2 (EGR2) expression. *J Biol Chem.* 2013;288(28):20488-20498.
25. Shan PF, Lu Y, Cui RR, Jiang Y, Yuan LQ, Liao EY. Apelin attenuates the osteoblastic differentiation of vascular smooth muscle cells. *PLoS One.* 2011;6(3):e17938.
26. Tang SY, Xie H, Yuan LQ, et al. Apelin stimulates proliferation and suppresses apoptosis of mouse osteoblastic cell line MC3T3-E1 via JNK and PI3-K/Akt signaling pathways. *Peptides.* 2007;28(3):708-718.
27. Schittny JC. Development of the lung. *Cell Tissue Res.* 2017;367(3):427-444.
28. Sanchez-Gurmaches J, Martinez Calejman C, Jung SM, Li H, Guertin DA. Brown fat organogenesis and maintenance requires AKT1 and AKT2. *Mol Metab.* 2019;23:60-74.
29. LaRocca J, Pietruska J, Hixon M. Akt1 is essential for postnatal mammary gland development, function, and the expression of Btn1a1. *PLoS One.* 2011;6(9):e24432.
30. Perez-Gil J, Weaver TE. Pulmonary surfactant pathophysiology: current models and open questions. *Physiology (Bethesda).* 2010;25(3):132-141.
31. Botas C, Poulain F, Akiyama J, et al. Altered surfactant homeostasis and alveolar type II cell morphology in mice lacking surfactant protein D. *Proc Natl Acad Sci U S A.* 1998;95(20):11869-11874.
32. Stahlman MT, Gray ME, Hull WM, Whitsett JA. Immunolocalization of surfactant protein-D (SP-D) in human fetal, newborn, and adult tissues. *J Histochem Cytochem.* 2002;50(5):651-660.
33. Wright JR. Immunomodulatory functions of surfactant. *Physiol Rev.* 1997;77(4):931-962.
34. Barclay AN, Ward HA. Purification and chemical characterisation of membrane glycoproteins from rat thymocytes and brain, recognised by monoclonal antibody MRC OX 2. *Eur J Biochem.* 1982;129(2):447-458.
35. Nie Y, Hu Y, Yu K, et al. Akt1 regulates pulmonary fibrosis via modulating IL-13 expression in macrophages. *Innate Immun.* 2019;25(7):451-461.
36. Crosbie PA, Crosbie EJ, Aspinall-O'Dea M, et al. ERK and AKT phosphorylation status in lung cancer and emphysema using nanocapillary isoelectric focusing. *BMJ Open Respir Res.* 2016;3(1):e000114.
37. Yoshimura K, Suzuki Y, Inoue Y, et al. CD200 and CD200R1 are differentially expressed and have differential prognostic roles in non-small cell lung cancer. *Oncoimmunology.* 2020;9(1):1746554.
38. Nishikiori H, Chiba H, Ariki S, et al. Distinct compartmentalization of SP-A and SP-D in the vasculature and lungs of patients with idiopathic pulmonary fibrosis. *BMC Pulm Med.* 2014;14:196.
39. Sorensen GL. Surfactant Protein D in Respiratory and Non-Respiratory Diseases. *Front Med (Lausanne).* 2018;5:18.
40. Piairo P, Moura RS, Baptista MJ, Correia-Pinto J, Nogueira-Silva C. STATs in Lung Development: Distinct Early and Late Expression, Growth Modulation and Signaling Dysregulation in Congenital Diaphragmatic Hernia. *Cell Physiol Biochem.* 2018;45(1):1-14.
41. Campbell CT, Kolesar JE, Kaufman BA. Mitochondrial transcription factor A regulates mitochondrial transcription initiation, DNA packaging, and genome copy number. *Biochim Biophys Acta.* 2012;1819(9-10):921-929.
42. Srivillibhuthur M, Warder BN, Toke NH, et al. TFAM is required for maturation of the fetal and adult intestinal epithelium. *Dev Biol.* 2018;439(2):92-101.

43. Lausen M, Lynch N, Schlosser A, et al. Microfibril-associated protein 4 is present in lung washings and binds to the collagen region of lung surfactant protein D. *J Biol Chem.* 1999;274(45):32234-32240.
44. Dieterle AM, Bohler P, Keppeler H, et al. PDK1 controls upstream PI3K expression and PIP3 generation. *Oncogene.* 2014;33(23):3043-3053.

FUNDING INFORMATION

NIGMS/NIH grant Number P30GM114750 and Oh–Zopfi Grant for Perinatal Research, Women & Infants Hospital of Rhode Island.

AUTHORS' CONTRIBUTIONS

TN participated to the conception and design of the study, performed the experiments, analyzed the data, conclude/summarize the study and wrote the manuscript. NA conducted the proteomics analysis and biocomputational analysis. RAE performed the image analysis including the morphological, immunohistochemistry quantification and densitometry analyses and edited the manuscript. AU and GT contributed advanced bio-computational analysis. LN prepared samples for LC-MS/MS analysis. JSE conceived and approved the study. All the authors read, revised and approved the final manuscript.

DATA AVAILABILITY STATEMENT

Proteomics dataset is submitted in public repository website at massive.uscd.edu. The accession number is MassIVE MSV 000086641.

Figure legends

Figure 1: Confirmation of pulmonary hypoplasia mouse model. (A) to (C) represent the effect of oligohydramnios on the morphometry of distal air space. (A) representative H & E stained histological sections (20x) showing a marked decrease in the air spaces in OH lungs when compared to UnT control, (B) binary image of the spaces from A and (C) analysis of the size of the spaces using the area and perimeter parameters showing a significant decrease of space size on OH (n= 6) in comparison to UnT (n= 5). (D) Representative western blots (blot of one replicate) showing the protein expression in OH lung compare to UnT. Name of the proteins were shown at the right side of the blot and corresponding molecular markers were shown at the left. T1 alpha and EMCN were down regulated and SP-C was unchanged compared to UnT lung. Vinculin served as endogenous control. Protein used in this assay was taken from the same samples used in proteomic analysis. *$p \leq 0.05$ and ****$p \leq 0.0001$

Figure 2: Comparative label-free quantitative proteomic analysis of hypoplastic (OH) and control fetal mouse lungs (UnT). Proteome from three biological replicates of each condition was subjected to quantitative analysis. (A) PCA analysis of total proteome dataset showed comparatively close clustering of total normalized protein abundance of the replicates in each condition, however distinct from other groups/condition. Samples are colored by experimental conditions in which orange and blue represent normal and pulmonary hypoplasia respectively. (B) shows the volcano plot analysis of the 3387 proteins subjected to the analysis. Significantly increased and decreased proteins in hypoplastic lungs compared to control lungs are marked as red and green, respectively. X-axis represents differentially expressed proteins with abundance by log2 ratio and Y-axis represents statistical significance with -log 10 of p value. Gray dots are non-significant ($p > 0.05$) and below the threshold of the fold change (1.5-fold). (C) shows the heat map clustering of total differentially expressed protein pattern of each groups. (D) a group of proteins showed very similar expression pattern in each condition in all three replicates regardless of

outliers (one replicate from each condition). R1, R2 and R3 denote three replicate experiments. One lung for each condition was taken from each replicate experiment in LC-MS analysis.

Figure 3: Gene enrichment pathway analysis of the significantly abundant proteins. Significantly increased (340) and decreased (134) proteins in hypoplastic lung compared with the control lungs are used in KEGG and Wiki pathways analysis as shown in (A) and (B) respectively. The red and dark green bar diagrams represent the increased and decreased proteins in hypoplastic lung respectively. Green circles indicate the number of genes identified in each pathway. Enrichment FDR p-value ≤ 0.05 was used in the analysis. The Analysis was conducted with an open source bioinformatics platform named Shiny GO (http://bioinformatics.sdstate.edu/ go/).

Figure 4: Quantification of protein expression in the lungs of fetal mice by western blot. Protein used in this assay was taken from the same pool as those were used in proteomic analysis. (A) and (B) represent immunoblotting and densitometric analysis respectively for the quantification of AKT1, AKT2, SP-D and CD200 proteins. Vinculin represents the loading control for endogenous protein. Western blot analysis showed decreased expression of AKT1 in OH lungs compare to UnT lungs whereas AKT2 was unchanged. The expression of SP-D and CD200 also showed significant reduction in OH lungs. repl.1, repl.2 and repl.3 denote three replicate experiments. n=3 per group. Densitometry analysis was performed for each target protein individually for three replicates relative to the mean of the UnT control and correspondence statistical significance were measured by t-test. *$p \leq 0.05$ & **$p \leq 0.01$.

Figure 5: Quantification of proteins in the tissue of fetal mice by IHC analysis. (A), (D) and (G) representative micrographic images of AKT1, SP-D and CD200 stained sections of lung tissue respectively. Left and right images (20x) are of negative control (for the detection of AKT1, SP-D, and CD200 respectively) and OH lung respectively. Middle represents the UnT lung of corresponding proteins. (B), (E) and (H) analysis of the DAB positive cells as automatically analyzed using QuPath. Positive cells are in

red. (C), (F) and (I) quantification of the images showed that the percentage of AKT1, SP-D and CD200 positive cells in OH-lung were significantly decreased compare to UnT lungs (upper bar diagram respectively). The mean intensity of the AKT1, SP-D and CD200 expressions in both nuclei and whole cells were also significantly reduced in OH lungs (lower bar diagram respectively). n=3 per group. *$p \leq 0.05$ & ****$p \leq 0.0001$. Arrows pointing to positive cells. Images in this figure are subsets of the original whole images (supplementary file 2). In (A) and (G) the brightness and contrast of the images were adjusted for publication purposes. The analyses were performed on the original untouched images. Images in (D) were captured with a different microscope as detailed in the methods.

Figure 6: Protein-protein interaction networks. A protein-protein interaction network was created using a total of 340 proteins those were significantly (1.5-fold, p-value < 0.05) decreased in abundant in OH induced hypoplastic lungs. Line color indicates the strength of the data support based on the experiments (pink line), co-expression (black line), gene-fusion (red line) and co-occurrence (blue line) according to the STRING (http://string-db.org/). Red rectangular marked proteins were further verified by immunoblot analysis. Figure was created by using BioRender.Com.

Figure 1

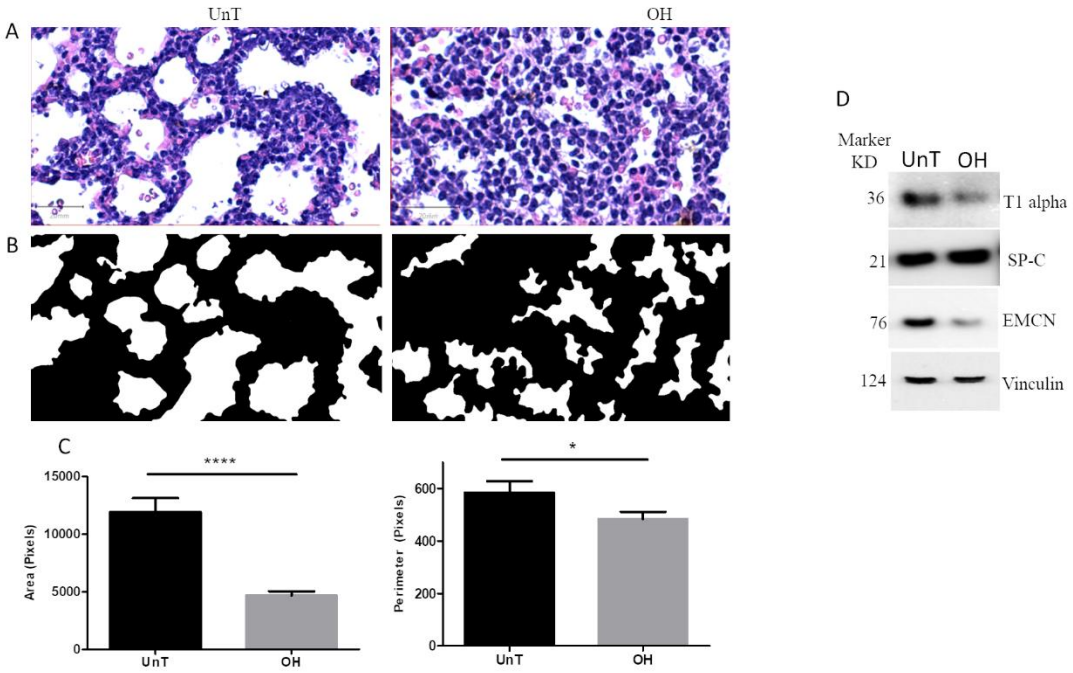

Figure 2

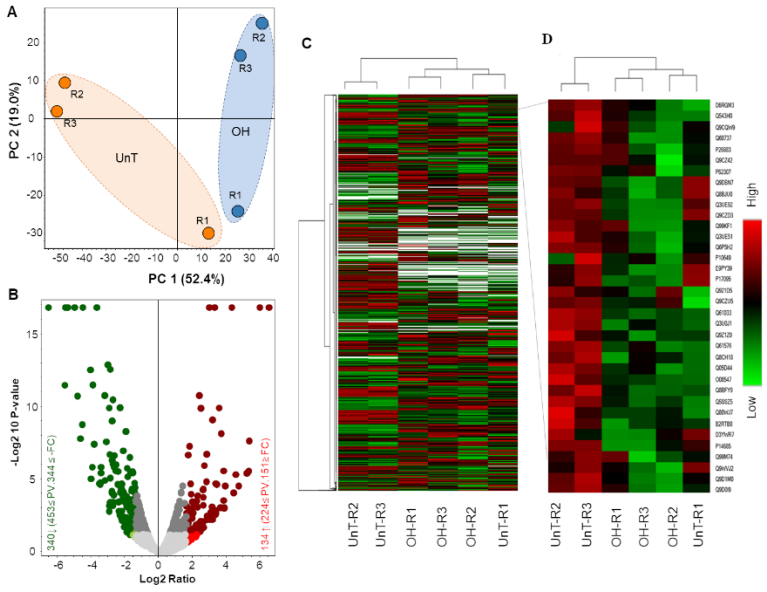

Figure 3

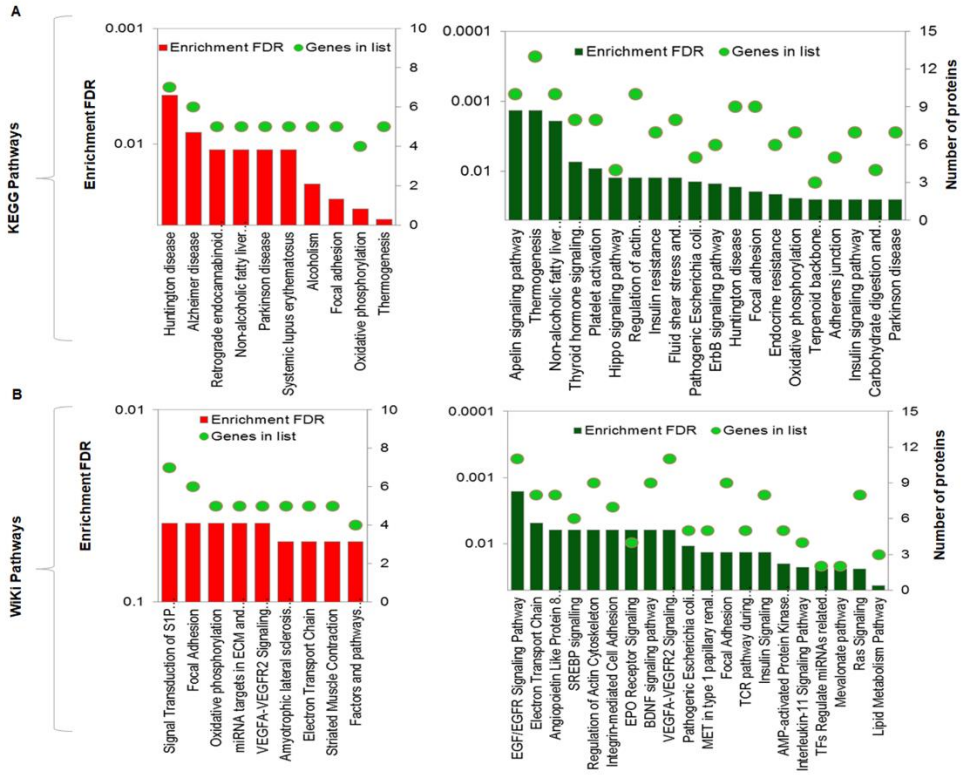
A
KEGG Pathways
Enrichment FDR
Enrichment FDR
Genes in list
0.001
0.01
10
8
6
4
2
0
Huntington disease
Alzheimer disease
Retrograde endocannabinoid...
Non-alcoholic fatty liver...
Parkinson disease
Systemic lupus erythematosus
Alcoholism
Focal adhesion
Oxidative phosphorylation
Thermogenesis
Enrichment FDR
Genes in list
0.0001
0.001
0.01
15
12
9
6
3
0
Number of proteins
Apelin signaling pathway
Thermogenesis
Non-alcoholic fatty liver...
Thyroid hormone signaling...
Platelet activation
Hippo signaling pathway
Regulation of actin...
Insulin resistance
Fluid shear stress and...
Pathogenic Escherichia coli...
ErbB signaling pathway
Huntington disease
Focal adhesion
Endocrine resistance
Oxidative phosphorylation
Terpenoid backbone...
Adherens junction
Insulin signaling pathway
Carbohydrate digestion and...
Parkinson disease
B
WiKi Pathways
Enrichment FDR
Enrichment FDR
Genes in list
0.01
0.1
10
8
6
4
2
0
Signal Transduction of S1P...
Focal Adhesion
Oxidative phosphorylation
miRNA targets in ECM and...
VEGFA-VEGFR2 Signaling...
Amyotrophic lateral sclerosis...
Electron Transport Chain
Striated Muscle Contraction
Factors and pathways...
Enrichment FDR
Genes in list
0.0001
0.001
0.01
15
12
9
6
3
0
Number of proteins
EGF/EGFR Signaling Pathway
Electron Transport Chain
Angiopoietin Like Protein 8...
SREBP signalling
Regulation of Actin Cytoskeleton
Integrin-mediated Cell Adhesion
EPO Receptor Signaling
BDNF signaling pathway
VEGFA-VEGFR2 Signaling...
Pathogenic Escherichia coli...
MET in type 1 papillary renal...
Focal Adhesion
TCR pathway during...
Insulin Signaling
AMP-activated Protein Kinase...
Interleukin-11 Signaling Pathway
TFs Regulate miRNAs related...
Mevalonate pathway
Ras Signaling
Lipid Metabolism Pathway

Figure 4

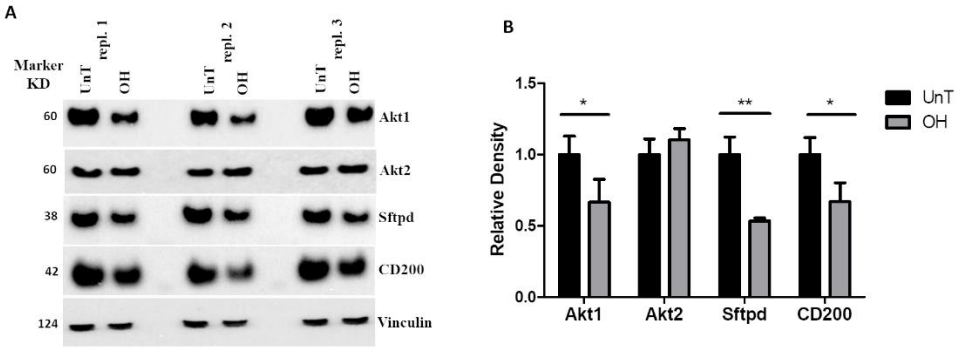
A
Marker KD
UnT
OH
repl. 1
repl. 2
repl. 3
60
Akt1
60
Akt2
38
Sftpd
42
CD200
124
Vinculin
B
Relative Density
1.5
1.0
0.5
0.0
*
**
*
UnT
OH
Akt1
Akt2
Sftpd
CD200

Figure 5

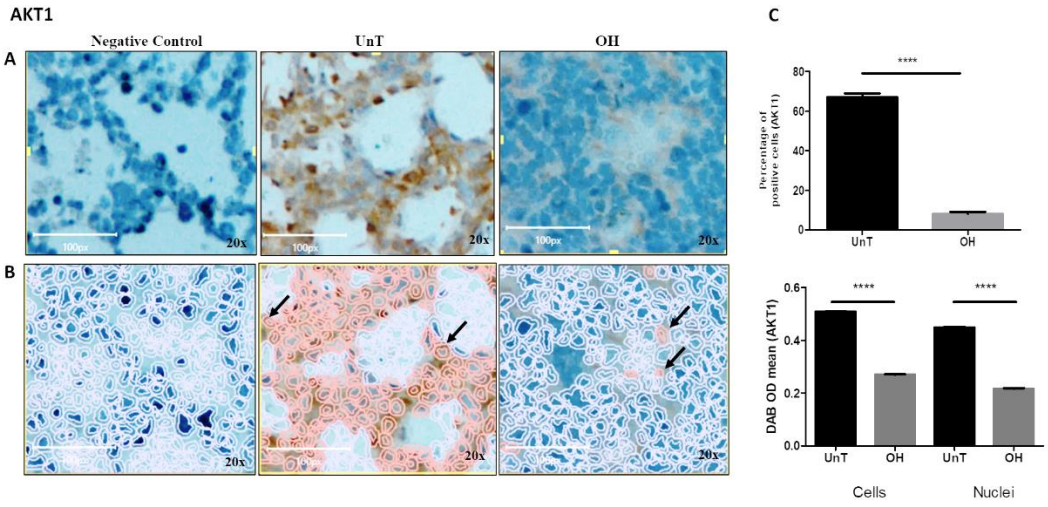
AKT1
Negative Control
UnT
OH
A
B
C
20x
100px
Percentage of positive cells (AKT1)
80
60
40
20
0
****
UnT
OH
DAB OD mean (AKT1)
0.6
0.4
0.2
0.0
****
****
UnT
OH
UnT
OH
Cells
Nuclei

Figure 5

SP-D

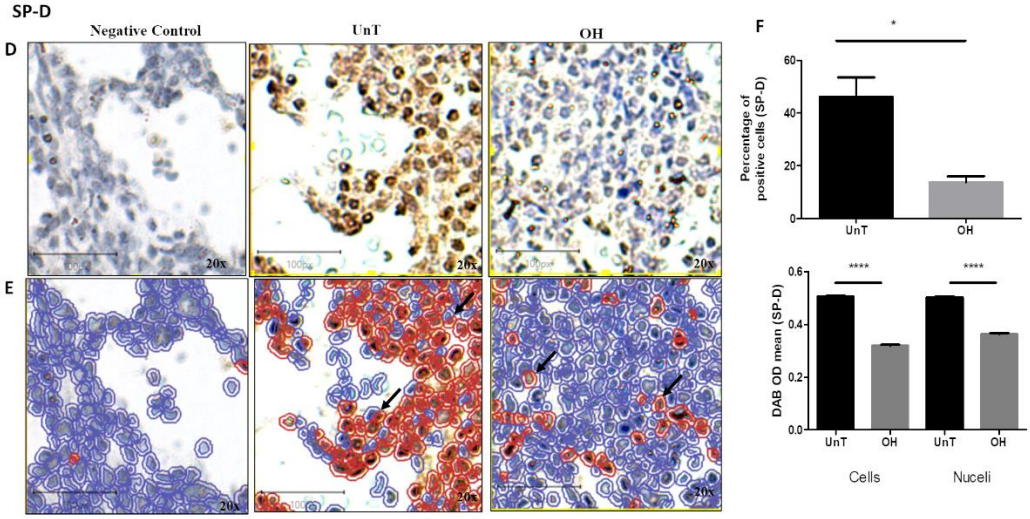
Negative Control
UnT
OH
D
E
20x
F
*
Percentage of positive cells (SP-D)
60
40
20
0
UnT
OH
****
****
DAB OD mean (SP-D)
0.6
0.4
0.2
0.0
UnT
OH
UnT
OH
Cells
Nuceli

Figure 5

CD200

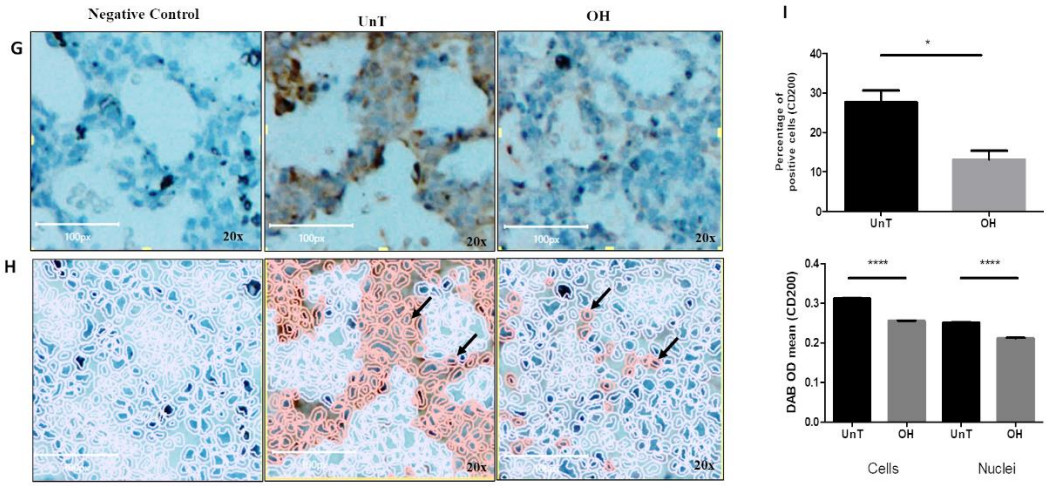

Figure 6

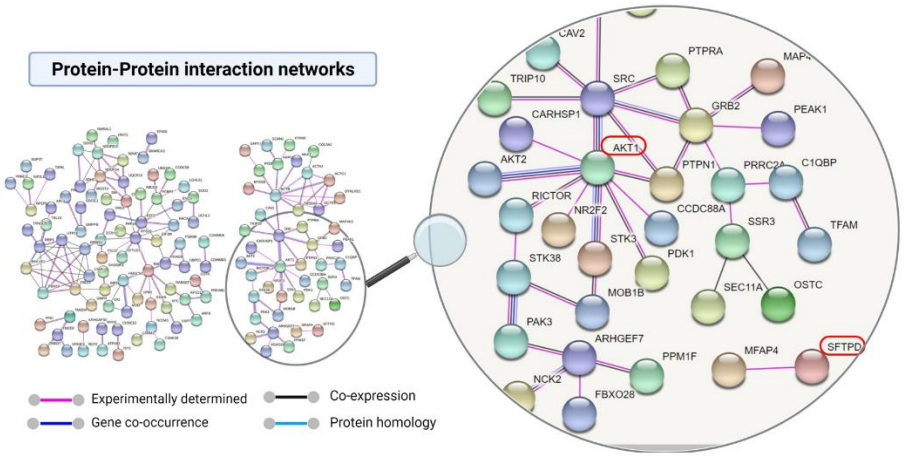
Protein-Protein interaction networks
CAV2
PTPRA
MAP4
TRIP10
SRC
GRB2
PEAK1
CARHSP1
AKT1
AKT2
PTPN1
PRRC2A
C1QBP
RICTOR
NR2F2
CCDC88A
SSR3
TFAM
STK3
PDK1
STK38
SEC11A
OSTC
MOB1B
PAK3
ARHGEF7
PPM1F
MFAP4
SFTPD
NCK2
FBXO28
Experimentally determined
Co-expression
Gene co-occurrence
Protein homology

Supplementary File 1

Detailed Materials and Methods

Animal Experiment to induce Oligohydramnios

Surgical procedures used in this study were approved by the Lifespan Institutional Animal Care and Use Committee (IACUC) of Rhode Island. We followed the procedure to induce pulmonary hypoplasia by OH as previously described (Najrana et al., 2017). Briefly, timed-pregnant Swiss Webster (SW) mice at E14.5 of gestation experienced median laparotomy under general anesthesia with isoflurane. The amniotic sacs from one uterine horn were punctured using a sterile $22^{1/2}$ -gauge needle to induce a rapid and abundant leakage of amniotic fluid. Fetuses at similar positions in the opposite horn served as controls. Four days after the surgery (at E18.5) fetuses were delivered by cesarean section. Right superior lobe of the lungs was collected and fixed overnight in 10% formalin, and the rest of the lungs were immediately frozen in liquid nitrogen and stored at -80°C. Fixed lungs were embedded in paraffin and tissue sections (5 µm in thickness) were placed on glass slides. Sections were stained with Hematoxylin and Eosin (H&E) or used for Immunohistochemistry (IHC) staining. Frozen lungs were submitted to COBRE Center for Cancer Research Development Proteomics Core Facility of Rhode Island Hospital, Providence, RI.

Sample preparation for proteomic analysis

Fetal mouse lungs were homogenized OH (n=3) and UnT (n=3) for 2 min at 5.5 m/s speed by Bead ruptor Elite (Kennesaw, GA) with a lysis buffer (8 M urea, 1 mM sodium orthovanadate, 20 mM HEPES, 2.5 mM sodium pyrophosphate, 1 mM ß-glycerophosphate, pH 8.0, 20 min, 4°C) and cleared by centrifugation (14 000 × g, 15 min, 15°C). Protein concentration was measured (Pierce BCA Protein Assay, Thermo Fisher Scientific, IL, USA) and a total of 200 µg of protein per sample was subjected to trypsin digestion. Tryptic peptides were desalted using C18 Sep-Pak plus cartridges (Waters, Milford, MA) and were lyophilized for

48 hours to dryness. The dried peptides were reconstituted in buffer A (0.1 M acetic acid) at a concentration of 1 µg/µl and 5 µl was injected for each analysis.

Lung Morphology Analysis

Digital images of the H&E stained sections of the lung were captured at 20x magnification using a Zeiss-Axio Imager upright microscope and an AxioCam MRC digital camera. These images were used to assess the area and perimeter of the lung spaces to confirm the pulmonary hypoplasia in the OH lungs. Analysis was performed as described [1]. Briefly, ImageJ (v 1.51r) (NIH, Bethesda, MD) was used to analyse the images (OH n=6, UnT n=5) by applying a Guassian Blur Filter (Sigma radius=4) to the green channel of the images. Otsu thresholding was then used to isolate the spaces [2] and the size of these spaces was assessed through measuring the area and perimeter [3].

Mass Spectrometry Analysis

The peptides were separated through a linear reversed-phase 90 min gradient from 0% to 40% buffer B (0.1 M acetic acid in acetonitrile) at a flow rate of 3 µl /min through a 3 µm 20 cm C18 column (OD/ID 360/75, Tip 8 µm, New objectives, Woburn, MA) for a total of 90 min run time. The electrospray voltage of 2.0 kV was applied in a split-flow configuration, and spectra were collected using a top-9 data-dependent method. Survey full-scan MS spectra (m/z 400-1800) were acquired at a resolution of 70,000 with an AGC target value of 3×10^6 ions or a maximum ion injection time of 200 ms. The peptide fragmentation was performed via higher-energy collision dissociation with the energy set at 28 normalized collision energy.

Antibodies

The following antibodies were used: anti- AKT1 antibody (clone C7H10)_host rabbit, Cell Signaling Tech, # 2938S; anti- AKT2 antibody (clone D6G4)_host rabbit, Cell Signaling Tech, # 3063; anti- SP-D antibody _host rabbit, Aviva system biological corporat, # OABF00765; Anti-Prosurfactant Protein C antibody, abcam # ab40879; Human/Mouse/Rat anti-CD200 antibody, R & D system, AF2724; Syrian hamster anti-

mouseT1α antibody, Hybrodoma Bank, # 8.1.1; goat anti-mouse endomucin antibody, R & D systems # AF4666; Peroxidase AffiniPure Donkey Anti-Rabbit IgG (H+L), Jackson Immuno Researcah, # 711-035-152; Rabbit IgG HRP-conjugated Antibody, R & D system, # HAF008; Goat IgG HRP-conjugated Antibody, R & D system, # HAF017; AffiniPure Goat Anti-Syrian Hamster IgG (H+L), Jackson Immuno Researcah, # 107-005-142.

Western blot

250 ng of lung tissue lysate was loaded on precast gel (NuPAGE 4-12% Bis-Tris Midi Gel, # WG1403BX10) and electrophoresis (Instrument: Invitrogen, XCell4 SureLockTM Midi-Cell) was done at 125 volts (Power supply: Bio-Rad, model no PowerPac HCTM, serial number 043BR05036) for 1.5 h using running buffer (NuPAGE # NP0002) followed by semidry-transfer (Instrument: Bio-Rad, model Trans-Blot® SD Cell, serial number 221BR 52475) on PVDF membrane at 16 volts (used above mentioned power supply) for 1 h at room temperature. 5% nonfat milk (Bio-Rad, # 170-6404) in 1 x PBS (Bio-Rad # 161-0780)) containing 0.1% tween-20 (blocking solution; Sigma # P2287-500 ML) was used to block the membrane for 1h at room temperature. The membrane was incubated with the primary antibody in blocking solution at 4° C overnight followed by incubation with HRP-conjugated secondary antibody in blocking solution for 1h at room temperature. Membrane was washed with PBS containing 0.05% of tween-20 for 45-60 min followed by chemiluminescent reagent (GE Healthcare, #RPN 2232) treatment and signal was detected on X-ray film. Densitometric analysis of the protein level was performed using ImageJ (v 1.51r) (NIH, Bethesda, MD).

Immunohistochemistry

The tissue was deparaffinized with citrus clearing solvent (ref. 8301, Thermo Scientific) and subsequently rehydrated with 100%, 95% and 75% alcohol. For immunohistochemistry (IHC), antigen retrieval was by incubating the tissue for AKT1 and SP-D in antigen unmasking solution (Vector, # H3301), for CD200 in antigen unmasking solution (Vector, # H3300) in the steamer (Hamilton Beach, type VS02, model 37537,

series A1721CU) for 25 mins and cooled down at room temperature for 20 min. Tissue sections were blocked in blocking solution (10% serum of species used to produce the secondary + 1% BSA + 1% Tween-20 (Sigma # P2287-500 ML) + 0.3 M glycine (solution in PBS) in 1 x PBS) for 1 hour at room temperature. Tissues were incubated overnight at 4° C with anti-AKT1 or anti-SP-D antibodies in blocking solution containing 0.1% Triton-x-100 (Sigma #T8532-500 ML), and with anti- CD200 antibody in blocking solution followed by incubation with 3% H_2O_2 (Fisher #H324-500) for 10 min at room temperature to eliminate the endogenous peroxidase activity. Tissue sections were incubated with HRP-conjugated secondary antibody in PBS containing 0.01% Triton-x-100 1 hour in room temperature. DAB (DAB substrate kit, cat. No. 550880, BD Pharmingen) staining and counter staining was done with hematoxylin (IHCWORLD, #IW-1400). Subsequently tissues were dehydrated with 75%, 95%, 100% alcohol and citrus clearing solvent and used cytoseal™ XYL (Ref. 83124, Thermo Scientific) to put coverslip on tissue. For quantification, 7-12 pictures representative from each quadrant of the sample were randomly chosen and photographed at 20x using a Zeiss-Axio Imager upright microscope and an AxioCam MRC digital camera for the SP-D. Nikon ECLISE 80i upright microscope and SPOT RT3 Color digital camera for AKT1 and CD200. Quantification of the positive cells was performed using QuPath software (0.2.0-m2) [4].

References

1. Najrana, T., et al., *Oligohydramnios compromises lung cells size and interferes with epithelial-endothelial development.* Pediatr Pulmonol, 2017. **52**(6): p. 746-756.
2. Otsu, N., *A threshold selection method from grey-level histograms.* IEEE Trans Syst Man Cybern, 1979. **9**(1): p. 62-66.
3. Landini, G., *Advanced shape analysis with imageJ*, in *The Second ImageJ User and Developer Conference*. 2008: Luxembourg. p. 116-131.
4. Bankhead, P., et al., *QuPath: Open source software for digital pathology image analysis.* Sci Rep, 2017. **7**(1): p. 16878.

Supplementary file 2

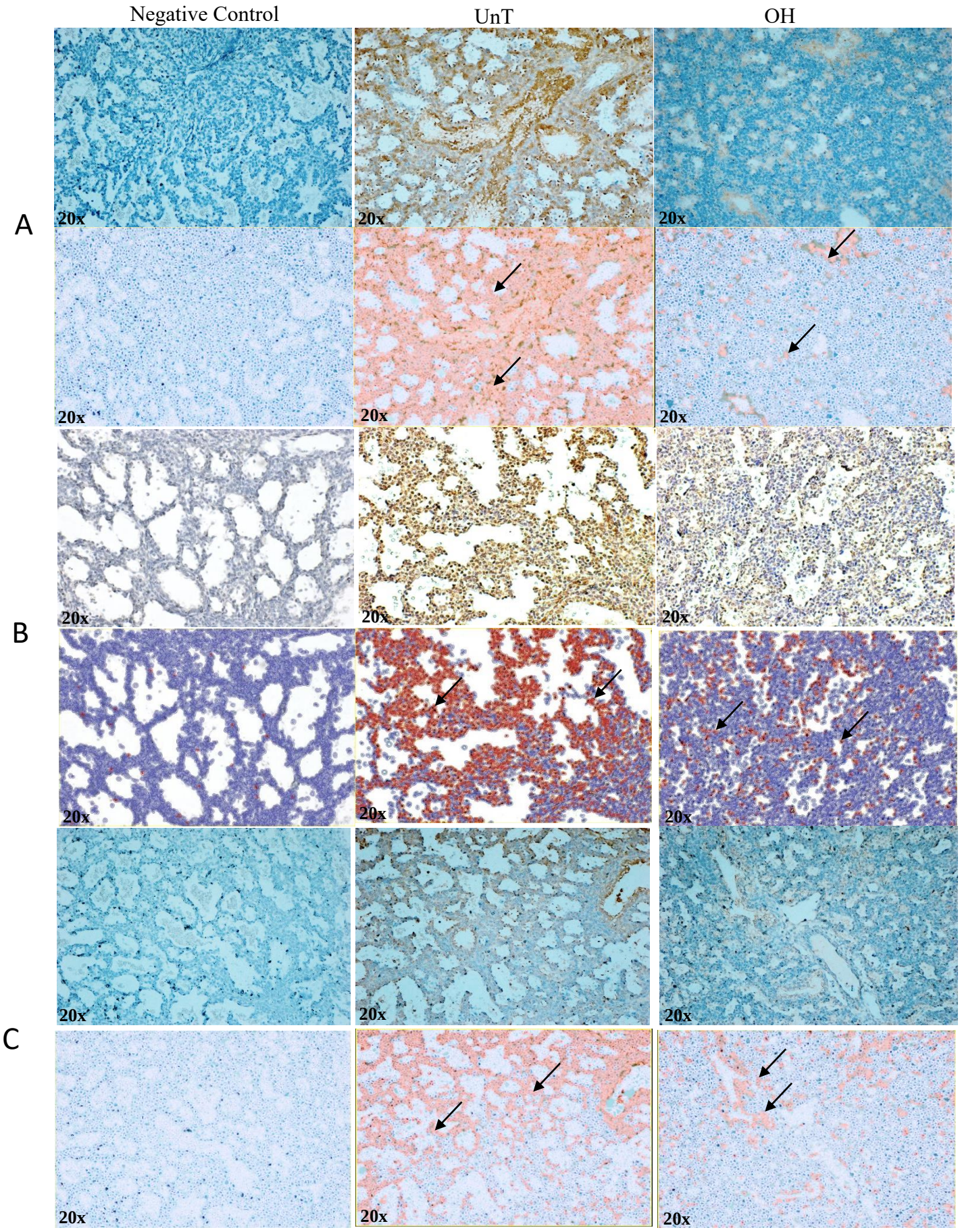

Supplementary data file 2: Quantification of proteins in the tissue of fetal mice by IHC analysis. Upper panel: (A), (B) and (C) representative micrographic images of AKT1, SP-D and CD200 stained sections of lung tissue respectively. Left and right images (20x) are of negative control and OH lung respectively. Middle represents the UnT lung of corresponding proteins. Lower panel (A), (B) and (C) analysis of the DAB positive cells as automatically analyzed using QuPath. Positive cells are in red. n=3 per group. *$p \leq 0.05$ & ****$p \leq 0.0001$. Arrows pointing to positive cells

In (A) and (C) the brightness and contrast of the images were adjusted for publication purposes. The analyses were performed on the original untouched images. Images in (B) were captured with a different microscope as detailed in the methods.

Supplementary data file 3A: Significant downregulated proteins

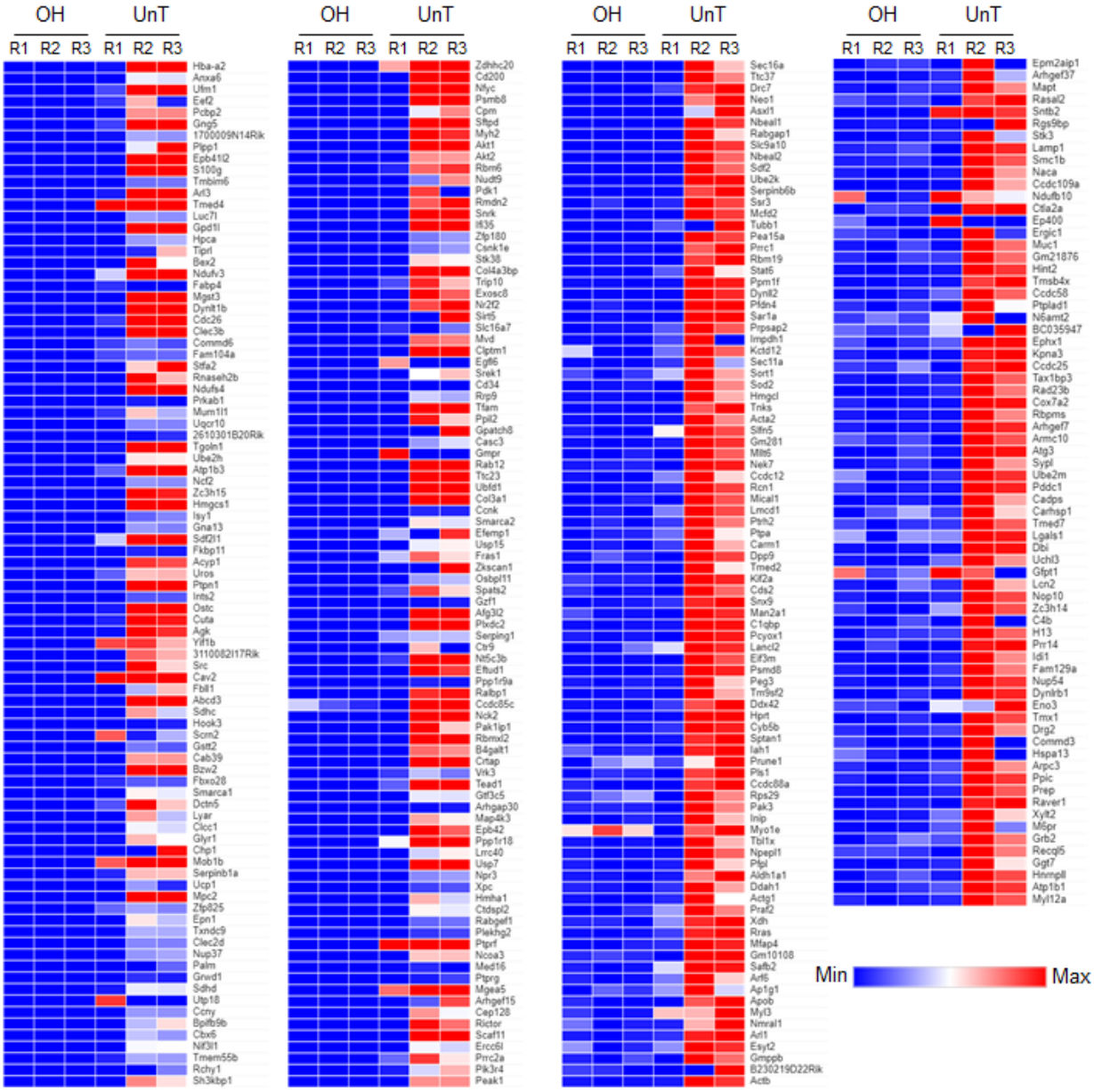

Supplementary data file 3B: Significant upregulated proteins

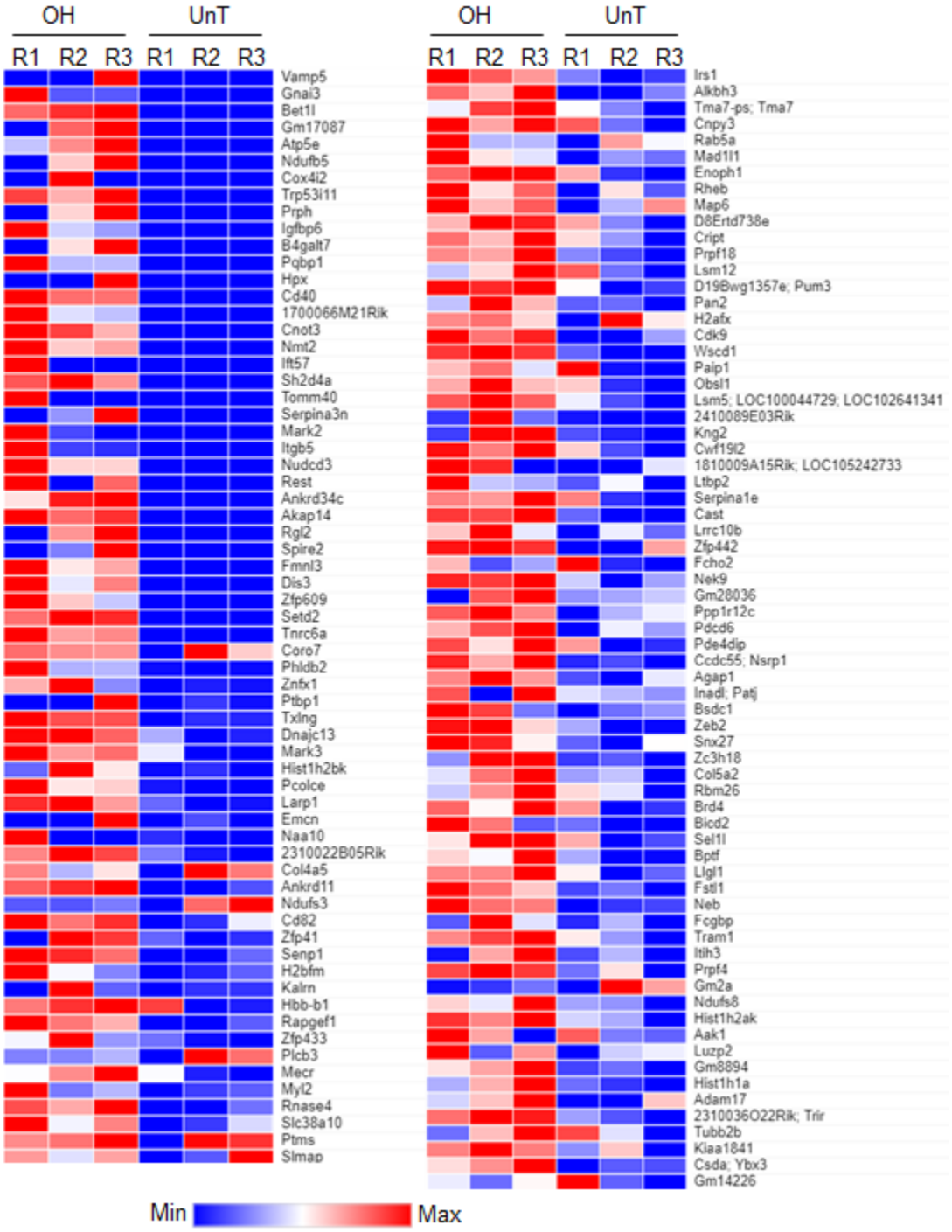

Supplementary data file 3: Heat maps providing the down and up regulated proteins lists. (3A) shows the heat map clustering of significantly down regulated protein pattern of each group. (3B) shows the

heat map clustering of significantly up regulated protein pattern of each group. R1, R2 and R3 denote three replicate experiments. One lung for each condition was taken from each replicate experiment.